This is the peer-reviewed, final accepted version for American Mineralogist, published by the Mineralogical Society of America.
The published version is subject to change. Cite as Authors (Year) Title. American Mineralogist, in press.
DOI: https://doi.org/10.2138/am-2022-8447. http://www.minsocam.org/

Word Count: 6897 (not including Table 1)

Revision 1

Incorporating previously neglected excess-oxygen associated with ferric iron in matrix corrections of microprobe data from cubic and rhombohedral Fe-Ti oxides

Michael A. Dungan[1], John J. Donovan[1], Andrew J. Locock[2], and Emma S. Bullock[3]

[1]Department of Earth Sciences, University of Oregon, OR 97403, USA, [2]Department of Earth and Atmospheric Sciences, University of Alberta, Edmonton, AB T6G 2E3, Canada, [3]Earth and Planets Laboratory, Carnegie Institution for Science, 5241 Broad Branch Rd. NW, Washington D.C., DC 20015, USA

Abstract

Estimates of the oxidation-states of magmas are important to current investigations of the geochemical characteristics of their source regions and of evolved magmatic series created during differentiation. One means of achieving such estimates is to capitalize on compositions of coexisting cubic and rhombohedral Fe-Ti oxides determined by electron microprobe. A combination of experimental calibration points and thermodynamic modelling provides a basis for translating such compositions into T-fO_2 values. This has been done until recently by estimating $Fe^{3+}/\Sigma Fe$ on the basis of charge balance and stoichiometry by the method of Droop

(1987), after matrix corrections of X-ray intensity data have been performed, as EPMA cannot be used routinely to distinguish different elemental valance states, much less accurately quantify abundances of Fe^{3+} and Fe^{2+}. The traditional approach of undertaking post-data-reduction calculations falls short of attaining the best possible quantitative results. The tactical choice of not accounting for light elements that have not been explicitly analyzed prior to matrix corrections of X-ray intensity data, leads to systematic errors in reported oxide abundances for measured elements. This article addresses one such issue, the oxygen associated with Fe^{3+} (hereafter "excess-oxygen"), on the basis of coexisting Fe-Ti oxides from Andean lavas. A new software routine in Probe for EPMA (hereafter PFE) uses an iterative calculation scheme to calculate amounts of excess-oxygen that would not be considered if all iron were assumed to be ferrous, and then applies this excess-oxygen during matrix corrections. The PFE approach reveals that Fe-concentrations have been underestimated, universally, in these minerals, because oxygen atoms absorb Fe *Kα* radiation: discrepancies increase as total Fe and Fe^{3+}/Fe^{2+}, hence excess-oxygen, increase. Analyses of the most Fe-rich cubic oxide compositions in this dataset have ~6 wt% excess-oxygen, and ~1 wt% more $FeO+Fe_2O_3$ than would be reported without incorporating the impact of excess-oxygen in matrix corrections. Minor to negligible differences in other elements are also observed. These effects are not because excess-oxygen is directly attributed to these elements, although some may be present in multiple valence states, as matrix corrections are undertaken on the basis of the conventional assumptions that they occur as Cr^{3+}, V^{3+}, Mn^{2+}, Mg^{2+}, Ca^{2+}, and Si^{4+}. Rather, variably small increases in total Fe propagate through the matrix corrections for other elements, and these differences may be recorded as minor increases or decreases in some concentrations, depending on the particular element and the

amount of change in Fe-concentration. $Fe^{3+}/\Sigma Fe$ in analyses produced with the PFE routine are essentially identical to those determined in the traditional mode, as cation proportions calculated on the basis of charge balance and stoichiometry, with the method of Droop (1987), is a necessary step. The new method: (1) provides more accurate concentrations, mainly for Fe and Ti, (2) is applicable to any mineral containing ferric iron (subject to stoichiometric constraints), (3) provides more accurate analytical totals, which can be advantageous for evaluating analytical quality, and (4) does not impact estimates of oxidation state. Oxygen fugacities and temperatures determined with the model of Ghiorso and Evans (2008) are essentially unchanged.

Key words: Fe-Ti oxides, T-fO_2, electron microprobe, analytical methods, matrix corrections

Introduction

Magmatic oxygen fugacity is an important intensive parameter because, to a large extent, it reflects $Fe^{3+}/\Sigma Fe$, which: (1) in some sense, is a proxy for key geochemical aspects of magmatic source regions, (2) plays a role in determining the stabilities of ferromagnesian silicate and oxide phases, and (3) is, therefore, a factor that influences liquid lines of descent. A number of different laboratory methods are used, ideally in combination, to assess the oxidation-states of erupted mafic to silicic magmas, but exploitation of coexisting Fe-Ti oxides is a frequently applied approach. If coexisting grains of the cubic phase (Fe_2TiO_4 - Fe_3O_4; hereafter spinel) and the rhombohedral phase ($FeTiO_3$ - Fe_2O_3) can be shown to be in equilibrium for Mg and Mn (Bacon and Hirschmann 1988), the compositions of such pairs are commonly used to calculate temperature and fO_2 (Ghiorso and Evans 2008). These results are often interpreted/presented as being equivalent to, or at least highly indicative of the oxidation-states of host magmas.

This is the peer-reviewed, final accepted version for American Mineralogist, published by the Mineralogical Society of America.
The published version is subject to change. Cite as Authors (Year) Title. American Mineralogist, in press.
DOI: https://doi.org/10.2138/am-2022-8447. http://www.minsocam.org/

This contribution exclusively addresses analytical and data-reduction tasks necessary for the acquisition of accurate electron microprobe analyses of spinel and rhombohedral oxides (commonly referred to as Mgt and Ilm) by considering the excess-oxygen associated with Fe^{3+} during matrix corrections. This was not done prior to the introduction of a new feature in Probe for EPMA (PFE) software (Donovan et al. 2021). Oxide compositions calculated with and without this additional step, for the same analytical dataset, are compared (Table 1). Corrections for X-ray absorption of Fe *Kα* radiation by this quantity of oxygen atoms, plus minor impacts on other ZAF correction factors (Bullock et al. 2020), result in higher reported iron. Corrected oxide sums increase as excess-oxygen, hence total Fe (Fe*) and Fe^{3+}/Fe^{2+}, increase in the target materials. Nonetheless, changes in calculated $Fe^{3+}/\Sigma Fe$ are negligible. The petrological implications of this dataset, plus several hundred additional analyses of Fe-Ti oxides and other minerals on samples from the same volcanoes, which are not reported here, will be presented in other publications. Applying the PFE routine: (1) provides more accurate analyses, including analytical totals, (2) spares analysts 'post-reduction' data-processing steps in spreadsheets, and (3) minimizes the potential for errors that might be introduced during external calculations. Analyses not initially collected and reduced with PFE may be recalculated with the free application CalcZAF, which is available on-line from:
https://probesoftware.com/download/CalcZAF.msi

Microprobe analyses and excess-oxygen in matrix corrections

Analytical conditions

Mineral chemistry data were obtained in the University of Oregon electron microprobe laboratory (Cameca SX-100), which is operated by the CAMCOR shared-user facility. Beam conditions on unknowns were 15 kilovolts and 50 nanoamps, and the beam was focused to the minimum diameter possible (<1 μm). Thirty nanoamps and 3 micrometers were used for standards. Durations of single-point analyses were ~2.75 minutes. These data were obtained during two five-day sessions (Blocks 4-5-6 and Block 7; original file names retained), during which a complete standardization was undertaken six or seven times per session. Minerals were used as standards for Fe (magnetite), Si (quartz), and Al plus Ca (plagioclase). Synthetic oxides, with undetectable levels of elemental impurities, served as standards for Cr, V, Mg, Mn, and Ti. Backgrounds for standards and unknowns were determined by the mean atomic number method (Donovan and Tingle 1996; Donovan et al. 2016). Counting times and selections of diffracting crystals for all elements were optimized for best results on the basis of experience with this instrument, with particular attention to Fe, Ti, Mg, and Mn. Many analytical points were located manually, but automated traverses were used on sufficiently large grains (~15-50 μm), and on standards. Some thin sections received carbon coats of excessive thickness, and data from these have been corrected by a coating-thickness correction method in Probe for EPMA.

Geological and analytical frameworks

These data were collected primarily for the purpose of determining T-fO_2 of basaltic to dacitic lavas from five late-Quaternary (<1Ma to historic eruptions), frontal-arc volcanoes located between 36-38.7°S in the Andean Southern Volcanic Zone (SVZ: 33.4-41.2°S), Chile. A very large majority of these are analyses of groundmass grains, which occur as intergrown sub-grains of spinel and rhombohedral oxide. Other analyses include those of spinel that are not

paired with rhombohedral oxide, plus inclusions of spinel that are present in pyroxene or olivine phenocrysts, and which are subtly or substantially different in composition from groundmass, particularly for Mg and Al. These are discussed below in the context of their consequences for the PFE data-reduction scheme.

After filtering of evidently compromised data, the remaining oxide pairs were tested for equilibrium coexistence on the basis of Mg-Mn systematics (Bacon and Hirschmann 1988) and were assessed for T-fO_2 conditions (Ghiorso and Evans 2008). Some pairs failed the Bacon and Hirschmann test, and others did not converge on an acceptable solution in the Ghiorso and Evans (2008) routine. Some pairs that passed these tests returned T-fO_2 estimates and values of TiO_2 activity that are outliers with respect to coherent clusters of estimates from the same samples. Some of these outliers are thought to be xenocrystic grains. A total of 1722 analyses were assessed (Electronic Appendix), regardless of whether or not such analyses are used for T-fO_2 estimates elsewhere, as this study is concerned only with analytical accuracy. Analytical uncertainties (one sigma) calculated by PFE for these results are (relative % for rhombohedral and cubic oxides, respectively): (1) Fe 0.24 and 0.18, (2) Ti 0.13 and 0.25-0.55, (3) Mg 0.2-0.5 and 0.4-1.5, (4) Mn 1.1-1.5 and 1.8-3.5, (5) V 3.5-8.5 and 1.1-1.6.

T-fO_2 reference frame

Temperatures and oxygen fugacities of oxide pairs are not quoted, or included in the Electronic Appendix, apart from four pairs used to directly compare the two data-reduction protocols (Table 1). Approximate T-fO_2 ranges are cited with reference to the nickel-nickel oxide oxygen-buffer assemblage (ΔNNO; i.e., one log-unit more oxidizing than NNO = NNO

+1) to provide context. These analyses provide T-fO_2 estimates that extend over significant ranges of ΔNNO and T. The ends of some linear to quasi-linear data-arrays in Figures 1, 2, and 3 are labeled as corresponding to either "high-fO_2" or "low-fO_2" to provide context for assessing these compositional trends. Absolute values of oxygen fugacity cannot be equated to positions along these arrays, as both T and fO_2 vary along oxygen-buffer curves, and data from natural minerals do not define perfectly correlated trends for T and fO_2.

Samples for Blocks 4-5-6

The analyzed oxide pairs in Blocks 4-5-6 are from evolved mafic to dacitic lavas (~52-69 wt% SiO_2; generally low Mg#s) from Nevado de Longaví (NLV in Table 1: 36.2°S, Rodríguez, et al. 2007; Sellés, et al. 2022), Nevados de Chillán (36.8°S), Lonquimay (37.45°S), and Llaima (37.8°S, Bouvet de Maisonneuve et al. 2012; Schonwalder-Angel et al. 2018), which are located in the northern portion of the Longaví-Calbuco segment of the Andean Southern Volcanic Zone (SVZ: 36.2-41.2°S). Calculated temperatures are typical of intermediate to silicic arc magmas (~1000-670°C), but oxidation-states include extraordinarily reduced values for subduction-related magmas in some late Holocene to Historic Lonquimay lavas, which extend down to ~NNO −1.7. Those from amphibole-bearing magmas of comparable age and SiO_2 at Nevado de Longaví range up to ~NNO +1.7. Some of the least-evolved samples from Nevado de Longaví also feature olivine phenocrysts that contain spinel inclusions with Cr, Al, and Mg that are much higher than groundmass spinel (hereafter Cr-Al spinel; chartreuse symbols, black outlines). Some andesitic samples from Longaví contain augite phenocrysts with magnetite-rich spinel inclusions that are in part higher in Mg and Al, but without substantially higher Cr, than groundmass spinel in the same samples. Unlike the inclusions in olivine, these lie directly

adjacent to and partly overlap with the groundmass population for many compositional parameters. Select examples of this type ("Mg+Al rich spinel") are highlighted in Figures (green symbols) for the purpose of comparisons between diagrams. Choices of highlighted analyses are somewhat arbitrary, and are based primarily on observations of a range of offsets from the main arrays that are defined by groundmass spinel compositions.

Samples for Block 7

The vast majority of these data were collected from groundmass grains in basaltic lavas of the Upper Placeta San Pedro sequence (UPSPS) of the Tatara-San Pedro complex (TSPC, 36°S, south end of Palomo-Tatara segment, SVZ; Dungan et al. 2001; Dungan and Davidson 2004; Costa and Dungan 2005). Analyses from three mafic andesites (two from Llaima, one from the TSPC) are included. The latter yield oxygen fugacities (~NNO to NNO −0.5) that fall near the middle of the range for Blocks 4-5-6. Oxygen fugacities for pairs in UPSPS lavas are ~NNO to NNO +1.95, but temperatures are relatively low (850-560°C) despite being hosted in basaltic compositions (~50-52.3 wt% SiO_2; Mg# ~54-63). The considerable petrologic complexities represented by UPSPS lavas, and by this oxide dataset, are addressed elsewhere.

Systematics of iron-titanium oxide mineral chemistry

Prior to discussing these results, it may be useful to review substitution schemes in the system FeO-TiO_2-Fe_2O_3, as they pertain to the cubic and rhombohedral series (summarized by Frost 1991), as natural compositions nominally lie along or near the ulvöspinel (Fe_2TiO_4) - magnetite (Fe_3O_4) and ilmenite ($FeTiO_3$) - hematite (Fe_2O_3) joins, respectively. Equilibria along

This is the peer-reviewed, final accepted version for American Mineralogist, published by the Mineralogical Society of America.
The published version is subject to change. Cite as Authors (Year) Title. American Mineralogist, in press.
DOI: https://doi.org/10.2138/am-2022-8447. http://www.minsocam.org/

these two binary series in the synthetic system are characterized exclusively by the coupled exchange reaction $Fe^{2+}Ti^{4} \rightleftarrows 2Fe^{3+}$, wherein wt% FeO* (total Fe as FeO) and mole fractions of Fe_3O_4 and Fe_2O_3 vary primarily in response to changes in T and fO_2. Variations of T and fO_2 are intrinsically coupled along univariant oxygen-buffer curves (i.e., as T decreases, log fO_2 becomes more negative). Comparably well-correlated T-fO_2 variations are not required for suites of natural oxide data, as these are not intrinsically constrained by oxygen-buffer assemblages.

Second-order differences between natural, coexisting cubic and rhombohedral oxides are preferential partitioning of Al, Cr, and V into Fe-rich spinel, and correspondingly higher Mg and Mn in coexisting rhombohedral oxide. Magnesiochromite is an extreme example for Mg, Cr, and Al in spinel. The dataset presented here is consistent with this partitioning behavior, over modest ranges and relatively modest to very low concentrations of Mg, Al, Cr, V, and Mn (Electronic Appendix). Variations in these non-ternary elements are, in addition, sensitive to the elemental compositions of the melts from which they crystallize, and to minerals and/or melts with which they ultimately equilibrate: they are not coupled to the degree that Fe^{2+}, Fe^{3+}, and Ti^{4+} are along binary joins in the ternary system.

Iron-titanium oxides contain negligible to small quantities of CaO and SiO_2. Analyses collected with electron-beam placements that are too close to oxide grain-margins in contact with silicate phases or apatite (sensitive to 3D grain-boundary geometry below the polished-section surface), or too near silicate or apatite inclusions, may record spuriously-high concentrations of these elements due to secondary fluorescence (Borisova et al. 2018). Analyses of the rhombohedral phase collected within 1-2µm of grain boundaries against magnetite-rich spinel are potentially subject to extraneous iron X-ray counts due to secondary fluorescence, depending on 3D grain-boundary geometry. Care was taken, within the limiting constraints of grain size, to

minimize the impacts of these phenomena, and some data from unusually coarse-grained intergrown oxides in samples Chill-19 and CH-9 were collected along traverses specifically to monitor these effects. Most of the analyses collected in this study report concentrations of CaO and SiO_2 that range from not-detected to <0.10 wt% SiO_2 and not-detected to <0.15 wt% CaO. Some higher values are reported, as some oxide grains may have higher concentrations, or perhaps the 3μm beam-diameter-setting used for standards was inadvertently applied. Scarce analyses with high values are retained in the Electronic Appendix, but analyses with >0.35 wt% SiO_2 and >0.30 wt% CaO are not included in Figures.

Consequences of the PFE routine for iron-titanium oxides

The original feature of this data-reduction scheme is estimation of the amount of oxygen required by Fe^{3+} (i.e., Fe_2O_3), on the basis of initially treating all the iron in the target as ferrous, and then iteratively calculating the optimal amounts of excess-oxygen and Fe^{3+} on the basis of charge balance and stoichiometry as part of the matrix-correction routine. This approach raises sums of oxides, FeO*, Fe_2O_3, FeO, and TiO_2 in reported analyses (Figs. 1, 2, and 3). These are presented graphically as delta-values (e.g., $\Delta FeO = FeO_{PFE} - FeO_{Droop}$). "Droop" concentrations were obtained by reducing the same X-ray-intensity data with the EPMA Excess-Oxygen option turned off, and then calculating Fe^{3+} in a spreadsheet, following Droop (1987). Values of Fe_2O_3 wt% returned by the PFE routine strongly correlate with calculated quantities of excess-oxygen. Values of $Fe^{3+}/\Sigma Fe_{PFE}$ and $Fe^{3+}/\Sigma Fe_{Droop}$ are essentially identical, as this ratio is constrained by a combination of stoichiometry and charge balance in both methods (Table 1).

Vanishingly small increases in MnO, V_2O_3, Cr_2O_3, and comparably minor decreases in MgO and Al_2O_3 are also observed for some analyses (Table 1, Electronic Appendix), but are not illustrated. Changes in non-ternary elements, which rarely exceed 0.01 wt% absolute (up to 0.03 wt%), are on the order of 1-3% of the amounts present, but are up to ~0.20 wt% TiO_2 for Fe-rich grains of rhombohedral oxide in the most highly oxidized samples ($\Delta TiO_2 \leq 0.11$ wt% TiO_2 in coexisting spinel; Figs. 3c-3d). The observed levels of concentration-change for non-ternary elements generated by the PFE data-reduction scheme are unlikely to be petrologically significant at the absolute concentration-levels recorded in this dataset, and are not substantially larger than analytical uncertainties. The consequences of this correction scheme for Cr_2O_3 and Al_2O_3 in Cr-Al spinel are modest (usually <0.4 wt%), in light of higher absolute concentrations due to lower iron. Only a few such grains have been assessed: consequences for grains that are more Mg-, Al-, and/or Cr-rich are not documented here.

Iron and excess-oxygen

The amounts of excess-oxygen calculated for this dataset range from ~0.5 wt% up to ~6.2 wt% in some analyses of high-Fe spinel. FeO* is well-correlated with quantities of excess-oxygen for cubic and rhombohedral oxides (Figs. 1a-1b). The larger ranges of FeO* and excess-oxygen for the Blocks 4-5-6 data reflect their greater range in T-fO_2. Far stronger positive correlations are observed for $Fe^{3+}/\Sigma Fe$ versus excess-oxygen because this ratio expresses increasing Fe^{3+} (Figs. 1c-1d), which is the crux of the PFE data-reduction scheme. Analyses of rhombohedral oxides in highly oxidized andesitic and dacitic samples (Blocks 4-5-6) overlap in terms of excess-oxygen (~2.4-3.9 wt%) and ΔFe_2O_3 (~0.30-0.58 wt%) with analyses of spinel from relatively reduced andesitic and dacitic samples (Figs. 1d and 2b), despite lower FeO* in

the rhombohedral phase (Fig. 1b). The exchange-reaction cited above results in well-correlated relationships between mineral compositions and excess-oxygen values, as long as mineral compositions nominally lie on or near their respective binary joins.

Non-ternary components

Departures from joins in the ternary system due to the presence of Mg (Fe^{2+}), Cr (Fe^{3+}), and Al (Fe^{3+}) lead to departures from arrays that would be observed in a strictly three-component system. The analyses shown in green in Figures 1, 2, and 3 have combined quantities of MgO (~2.1-3.9 wt%) and Al_2O_3 (~2.1-5.3 wt%) that are higher than those in analyses that lie along the axes of nominal cubic and rhombohedral arrays. Selections of highlighted analyses are at some level arbitrary, as these are part of a continuum with data deemed to be part of the cubic array, and were made for the purposes of illustrative comparisons between multiple figures. All these spinel grains, and some others with lower MgO and Al_2O_3, occur as inclusions in pyroxene phenocrysts. MgO and Al_2O_3 define a weak positive correlation, but these non-ternary substitutions are not nearly as strongly coupled as are Fe^{2+}-Ti^{4+}-Fe^{3+}. Increasing MgO+Al_2O_3 correlates negatively with FeO* (Fig. 2d), but positively with Fe_2O_3 and Fe^{3+}/Fe*. These cubic oxides are Cr-poor (0.06-0.96 wt% Cr_2O_3) in comparison to Cr-Al spinel compositions in Fo-rich olivine phenocrysts (~4.7-16.7 wt%). Spinel inclusions in pyroxene overlap in terms of Cr-concentrations with groundmass spinel (0-0.53 wt% Cr_2O_3), but a large majority of the latter have <0.10 wt%.

Vanadium, which is assumed to be V^{3+} for the purpose of calculating excess-oxygen, is also a potential factor in reducing Fe^{3+} in spinel, but is much lower in rhombohedral oxides (not-

detected to 0.27 wt%, generally <0.15 wt%). Concentrations of V_2O_3 in spinel inclusions in pyroxene (~0.48-0.70 wt%) are positively correlated with MgO and Al_2O_3 in this restricted set of analyses, but not with FeO*. This limited range of concentrations falls near the middle of the wider range for groundmass spinel in Block 4-5-6 (0.13-0.96 wt% V_2O_3), wherein weak positive correlations with FeO* and Fe^{3+}/Fe^* and weak negative correlations with MgO and Al_2O_3 are observed. These relations are complicated by a range of calculated T-fO_2 values in combination with the high probability that V is present in multiple valence states, the proportions of which are largely controlled by oxygen fugacity (e.g., Canil and Fedortchouk 2001).

Cumulative effects of modest amounts of substitutions such as $Al^{3+} \leftrightarrows Fe^{3+}$, $Cr^{3+} \leftrightarrows Fe^{3+}$, and $Mg^{2+} \leftrightarrows Fe^{2+}$ in spinel are manifested by corresponding decreases in FeO* and excess-oxygen (Fig. 1b). This diffuse array has a nominally steeper trend than the orientation of the sub-parallel cubic and rhombohedral arrays (lower rate of change in excess-oxygen and higher rate for FeO*), because $Mg^{2+} \leftrightarrows Fe^{2+}$ is dominant over substitutions for Fe^{3+}. The Cr-Al spinel data (chartreuse/black outline) define a trend that is characterized by a substantial decrease in FeO* relative to magnetite-rich spinel, and which is correlated with decreasing excess-oxygen, due to a high rate of substitution of Cr and Al for Fe^{3+}. Even so, the Cr-Al spinel analyses display a much lower rate of decreasing $Fe^{3+}/\Sigma Fe$ relative to decreasing excess-oxygen, in comparison to the binary arrays, due in part to higher MgO (~4.1-5.5 wt%; Fig. 3d). Overlapping compositional fields in Figures 1b, 1d, 2b, 2d, and 2f for rhombohedral oxides from the most oxidized Nevado de Longaví samples and the spinel inclusions with the highest Al_2O_3 and Cr_2O_3 are fortuitous.

If analyses of extremely Al-rich spinel, such as those present in high-Fo olivine in high-T primitive basalts or spinel peridotites, were present on these plots, spinel data-trends related to increasing Cr+Al+Mg would continue toward minimal values of excess-oxygen and lower FeO*;

i.e., values of excess-oxygen for $MgAl_2O_4$, $MgCr_2O_4$, $FeCr_2O_4$, and $FeAl_2O_4$ = 0.00 wt%. Analyses of rhombohedral oxides are higher in MgO (~0.8-5.5 wt%; highest values from three low-outlier analyses from one sub-grain) in comparison to coexisting spinel (~0.2-2.5 wt%). Preferential partitioning of Mg into rhombohedral oxide ($Mg^{2+} \leftrightarrows Fe^{2+}$) leads to trivially lower values of excess-oxygen. Higher Al_2O_3 in coexisting spinel ($Al^{3+} \leftrightarrows Fe^{3+}$) results in proportionally greater reductions in excess-oxygen.

Differences in reported Fe^{2+} and Fe^{3+} between two data-reduction schemes

The functionally most important difference between the PFE routine and the method of Droop (1987) is that absolute concentrations of FeO*, FeO, and Fe_2O_3 are increased by PFE, and analytical sums of oxides increase accordingly (Table 1 and Electronic Appendix). Fe_2O_3 is up to ~0.6 wt% higher in magnetite-rich spinel with high $Fe^{3+}/\Sigma Fe$, and FeO wt% increases by up to ~0.35 in the same analyses. These results are intrinsically more accurate, because matrix corrections for all elements are being applied simultaneously and comprehensively. Both approaches require that sums of cations pfu and oxygen atoms pfu are 3.000 and 4.000 for cubic oxides and 2.000 and 3.000 for rhombohedral oxides. The absence of differences in $Fe^{3+}/\Sigma Fe$ between these two methods, for a given analysis, is the consequence of calculating this ratio on the basis of stoichiometry and charge-balance; i.e., additional Fe is partitioned between Fe^{3+} and Fe^{2+} according to these requirements. Estimates of ΔNNO and Fe-Ti closure-temperature calculated with the Ghiorso and Evans (2008) routine are essentially identical (Table 1).

The apparent separation of the Block 7 cubic and rhombohedral oxide analyses into mutually-exclusive, quasi-linear arrays for both parameters in Fig. 2a is characteristic of the

distributions observed in most plots of Block 7 data. The wider compositional ranges of oxides and associated oxygen fugacities for Block 4-5-6 data provide a more complete perspective. Low values of ΔFe_2O_3 are virtually identical between these two groups for rhombohedral oxides with <21 wt% Fe_2O_3, both of which are characterized by low ΔNNO. The extension of the rhombohedral array for Block 4-5-6 to ~38 wt% Fe_2O_3 for pairs in highly oxidized magmas (Nevado de Longaví) shows that compositions with lower ΔFe_2O_3 and lower excess-oxygen (Fig. 1d) for pairs in reduced Chillán and Lonquimay magmas are a high-TiO_2 extension of a curved distribution that becomes asymptotic to $\Delta Fe_2O_3 = 0$ as Fe_2O_3 wt% decreases toward zero ($FeTiO_3$). These trends would come close to intersecting the origins in both Figs. 1c and 1d in cases where the amounts of Fe_2O_3 and excess-oxygen were to become negligible. Compositions of low-Fe_2O_3 spinel from Lonquimay and Chillán extend this comparably curved array to low values of ΔFe_2O_3, which also would become negligible, as would excess-oxygen, in cases where cubic-oxide compositions were to approach pure ulvöspinel (Fe_2TiO_4; FeO = 64.27 wt%).

The Block 4-5-6 data (ΔNNO −1.7 to +1.7) demonstrate that the quasi-linear cubic and rhombohedral arrays manifested by the Block 7 data (ΔNNO −0.5 to +1.2) provide a somewhat simplified perspective with respect to the full consequences of the PFE data-reduction scheme. Block 4-5-6 analyses that 'fill the gap' between arrays in Block 7 data show that these distributions are extensions of parabolic curves radiating from points of origin that coincide with Fe_2O_3, ΔFe_2O_3, $Fe^{3+}/\Sigma Fe$, and excess-oxygen = 0.00. FeO* wt% decreases as a function of increasing $Fe^{3+}/\Sigma Fe$; i.e., as mole fractions of Fe_3O_4 and Fe_2O_3 increase, respectively. These relationships are illustrated by similarities between plots of FeO versus ΔFeO (Figs. 2c-2d; note offsets in y-axis scales) and FeO versus excess-oxygen (Figs. 2e-2f; note offsets in y-axis scales), which are inverse to the trends defined by Fe_2O_3 versus ΔFe_2O_3 (Figs. 2a-2b) and $Fe^{3+}/\Sigma Fe$

This is the peer-reviewed, final accepted version for American Mineralogist, published by the Mineralogical Society of America.
The published version is subject to change. Cite as Authors (Year) Title. American Mineralogist, in press.
DOI: https://doi.org/10.2138/am-2022-8447. http://www.minsocam.org/

versus excess-oxygen (Figs. 1c-1d). The tendency for these curves to accurately project towards Fe^{3+}-free end-member compositions, or alternatively toward Fe_3O_4, lends support to the reliability of the PFE calculation scheme.

Variations in TiO_2

Strong correlations, along the cubic and rhombohedral oxide arrays, between decreasing wt% TiO_2 versus increasing excess-oxygen (Figs. 3a-3b) and increasing $Fe^{3+}/\Sigma Fe$ (Figs. 3c-3d) are fully consistent with relations shown in Figures 1 and 2 (e.g., Figs. 1c-1d): as $Fe^{3+}/\Sigma Fe$ increases, TiO_2 must decrease, along with FeO, due to coupled substitutions. The application of matrix-corrections to Ti in the presence of abundant Fe, and variable excess-oxygen, creates complexities in TiO_2-variability that are not observed when the impact of the PFE routine is considered exclusively with respect to iron. Such complexities are discussed first with regard to Mg- and Al-rich magnetite inclusions in pyroxene and Cr-Al spinel, and then as they are manifested differently by ΔTiO_2 along the cubic and rhombohedral oxide arrays (Figs. 3c-3d).

Offsets of data points from relatively Mg- and Al-rich magnetite and Cr-Al spinel inclusions, away from the groundmass spinel array in Fig. 3b, are analogous to those manifested in Fig. 1d: excess-oxygen and TiO_2 decrease as functions of increasing non-ternary components. Strongly coupled substitutions along the spinel array are 'disrupted' by non-ternary elements in such a way as to create small, but apparently contrary offsets toward some combination of seemingly higher TiO_2 (Fig. 3d) and higher $Fe^{3+}/\Sigma Fe$ (Fig. 1d) for spinel inclusions in pyroxene, due mainly to $Mg^{2+} \leftrightarrows Fe^{2+}$, which increases $Fe^{3+}/\Sigma Fe$ and lowers excess oxygen (Fig. 1d). Still larger decreases in excess oxygen, and rapidly decreasing FeO*, are observed for the Cr-Al

This is the peer-reviewed, final accepted version for American Mineralogist, published by the Mineralogical Society of America.
The published version is subject to change. Cite as Authors (Year) Title. American Mineralogist, in press.
DOI: https://doi.org/10.2138/am-2022-8447. http://www.minsocam.org/

spinel data due to substitution of Fe^{3+} by Cr and Al (Fig. 1b). The positions of data points to the left of the groundmass spinel array in Fig. 1d give the impression that the primary consequence of these substitutions is lower excess oxygen, hence lower ΔFe_2O_3 and ΔTiO_2 (Figs. 1d, 2b, and 3d), however, $Fe^{3+}/\Sigma Fe$ and Fe_2O_3 in such compositions are also functions of $Mg^{2+} \leftrightarrows Fe^{2+}$, $Fe^{3+} \leftrightarrows Al^{3+}$, and $Fe^{3+} \leftrightarrows Cr^{3+}$. These multi-element relationships are a reminder that the PFE routine is based on matrix corrections for all of the elements in an analytical dataset, hence on calculated values of excess-oxygen and Fe^{3+}.

Further indications of the sensitivity of corrected wt% TiO_2 in the PFE calculation are the distributions observed for ΔTiO_2 versus wt% TiO_2 (Figs. 3c-3d). The relatively limited ranges of $Fe^{3+}/\Sigma Fe$ in the Block 7 cubic and rhombohedral arrays (Fig. 3c) yield slightly curved trends for both series. However, unlike ΔFeO and ΔFe_2O_3, for which maximum delta-values are obtained from pairs that record the highest oxidation-states, the highest ΔTiO_2 along the spinel array is manifested by grains from the least oxidized samples. Analyses of spinel in pairs that record high-fO_2 oxidation-states define a curved trend that projects toward 0.00 wt% TiO_2 and $\Delta TiO_2 = 0$. The low-fO_2 end of the rhombohedral oxide array projects to ~52-53 wt% TiO_2, which is the composition of end-member ilmenite (52.64 wt%). The opposing polarities of ΔTiO_2 are consistent with coupled TiO_2-variations along these two solid-solution series.

Additional insights into the PFE routine are evident in the Blocks 4-5-6 dataset (Fig. 3d; note change in x-axis scale from 3e), which records wider compositional ranges due to a greater range in ΔNNO. The trend that characterizes the spinel array at low fO_2, wherein TiO_2 exceeds ~16 wt% and $Fe^{3+}/\Sigma Fe < 0.44$ (excess-oxygen <3.6 wt%) is relatively low, is informative. These analyses (Chillán and Lonquimay) define a curved trend, along which ΔTiO_2 begins to decrease as TiO_2 increases above ~16 wt%. This can be understood through a virtual parabola that would

This is the peer-reviewed, final accepted version for American Mineralogist, published by the Mineralogical Society of America.
The published version is subject to change. Cite as Authors (Year) Title. American Mineralogist, in press.
DOI: https://doi.org/10.2138/am-2022-8447. http://www.minsocam.org/

connect the compositions of pure Fe_3O_4 (wt% TiO_2 = 0.00) and pure Fe_2TiO_4 (35.73 wt% TiO_2), both of which would be characterized by excess oxygen and ΔTiO_2 = 0.00. The curve joining these obligatory termination points can be constructed only on the basis of analyses of spinel in the ternary system, but it can be inferred to extend to ~ΔTiO_2 ~0.12 wt% at ~15-17 wt% TiO_2. The position of this curve would not coincide precisely with the data-array due to the consequences of non-ternary substitutions. The maximum observed ΔTiO_2 in spinel (+0.105 wt%) is of negligible importance, and this would diminish with increasing fraction of ulvöspinel. Relative increases in ΔTiO_2 are also minor for the rhombohedral phase, and only approach +0.2 wt% (~0.5% relative) for high-$Fe^{3+}/\Sigma Fe$ compositions with ~40 wt% TiO_2.

Implications

With rare exceptions, terrestrial iron-titanium oxide and aluminous spinel grains contain both ferrous and ferric iron. Pure hematite is an exception, but all the oxygen associated with Fe^{3+} still needs to be included in matrix corrections to yield the best results (Bullock et al. 2020). The likelihoods of terrestrial end-member ilmenite or ulvöspinel occurring outside an experimental laboratory, or of Fe^{3+}-free Cr-Al spinel occurring naturally, are vanishingly low. Some rock-forming silicate minerals, such as amphibole, garnet, mica, and pyroxene, also contain both ferrous and ferric iron, partly as functions of the large range of oxidation states present in terrestrial geological environments. Petrologic studies of magmatic processes frequently depend on indirect estimates of the quantities of Fe^{2+} and Fe^{3+} that are present in natural and experimental minerals and glasses to interrogate the role of oxidation-state in determining mineral stabilities, liquid lines of descent, and source-region chemistry.

This is the peer-reviewed, final accepted version for American Mineralogist, published by the Mineralogical Society of America.
The published version is subject to change. Cite as Authors (Year) Title. American Mineralogist, in press.
DOI: https://doi.org/10.2138/am-2022-8447. http://www.minsocam.org/

The electron microprobe is a cumbersome tool for quantitatively resolving X-rays emanating from Fe^{2+} and Fe^{3+} (c.f., Höfer and Brey 2007; Zhang et al. 2018). A widely used approach for estimating $Fe^{3+}/\Sigma Fe$ during routine analyses has been to calculate a putative fraction of Fe^{3+} on the basis of charge balance and stoichiometry (Droop 1987). A flaw in this methodology is that the absorption of iron X-rays by oxygen is inevitably underestimated by virtue of the initial simplifying assumption, that $Fe^* = Fe^{2+}$, prior to matrix corrections, thereby excluding the amount of oxygen related to Fe^{3+} content (herein, excess-oxygen) from these corrections. An additional data-reduction step, which is operational in Probe for EPMA software, seamlessly implements a second level of matrix corrections that incorporate 'found' quantities of oxygen by iteratively optimizing $Fe^{3+}/\Sigma Fe$ and the quantity of calculated total oxygen under the constraints of stoichiometry and charge balance. This approach increases sums of oxides by recalculating amounts of FeO*, Fe_2O_3, FeO, and TiO_2 (decreasing order of amounts added). $Fe^{3+}/\Sigma Fe$ remains essentially unchanged, but oxide concentrations are reported more accurately. Titanium is a major constituent of iron-titanium oxides, and other transition-element metals such as V, Cr, Mn, Ni, Cu, and Zn, plus Nb in ilmenite, may be present in negligible to substantial quantities in both Mg-rich, aluminous spinel and iron-titanium oxides (Electronic Appendix). The impact of excess-oxygen on all analyzed elements is included in matrix corrections by the PFE software routine during on-line data-reduction.

A dataset comprised mainly of analyses of coexisting cubic and rhombohedral groundmass grains, which lie near the binary Fe_2TiO_4-Fe_3O_4 and $FeTiO_3$-Fe_2O_3 joins in the system FeO-TiO_2-Fe_2O_3, has been used to illustrate the practical implications of the PFE data-reduction algorithm. This provides a systematic basis for assessing the consequences of capitalizing on values of calculated excess-oxygen to improve analytical accuracy. The Fe-Ti

oxides are particularly informative in this regard because first-order compositional variations along both joins are related to the same coupled substitution-scheme (i.e., $Fe^{2+}Ti^{4+} \rightleftarrows 2Fe^{3+}$).

Analyses of spinel inclusions hosted by pyroxene and olivine in some samples have variably-higher amounts of non-ternary elements such as Mg, Al, and Cr (among others that are present at generally low concentrations), which are not nearly as rigorously coupled as are Fe^{2+}-Ti^{4+}-Fe^{3+}. These serve as examples of the consequences for data-reduction of second-order substitutions in Fe-rich spinel, and of substitution-schemes in Mg-Cr-Al-Fe spinel, which lack the constraint of lying along a binary join, and are variably non-ideal (e.g., Sack and Ghiorso 1991a and 1991b). Reductions in amounts of FeO and Fe_2O_3 related to increased non-ternary substitutions diminish quantities of calculated excess-oxygen and the degree to which PFE-determined concentrations differ from those reported without considering excess-oxygen.

The ratio $Fe^{3+}/\Sigma Fe$ is among the most important parameters that factor into T-fO_2 values derived from compositions of coexisting cubic and rhombohedral oxide pairs in igneous and metamorphic rocks (Ghiorso and Evans 2008). The ongoing dependence on charge balance and stoichiometry for calculating Fe_2O_3 provides continuity between values of $Fe^{3+}/\Sigma Fe$ obtained without excess-oxygen by the traditional application of the method of Droop (1987) and those by the revised PFE-method, wherein excess-oxygen is considered (Bullock et al. 2020; Fournelle et al. 2020). The assumptions on which the method of Droop (1987) is based become increasingly tenuous as mineral structural formulae and compositions become less rigidly constrained by virtue of undetermined and/or potentially non-stoichiometric amounts of OH, H_2O, halogens, or other light components (Fournelle et al. 2020). High-temperature Fe-Ti oxides are not known to contain appreciable quantities of hydroxyl, water, carbon dioxide, or halogens, and it is equally

unlikely that Li, B, Be, or N are present in amounts sufficient to quantitatively impact the assumptions that underpin the Droop (1987) equations.

Explicit determinations of oxygen abundances during 'routine' analyses of Fe-Ti oxides and Mg-Cr-Al-Fe-Ti spinel could, in principle, improve the accuracy of calculated Fe_2O_3 (e.g., Nash 1992). However, researchers would be forced to 'significantly' increase the durations of analyses in order to obtain data for oxygen at the level of precision that would be required to improve on calculations of excess-oxygen and Fe^{3+} by the PFE routine. The latter elevates the quality of analytical results relative to previous practices, without increased analysis times, without additional sample-preparation steps, and without a need for technological advances beyond the current analytical state-of-the-art.

Acknowledgements We thank Julie Chouinard, Steve Wiemholt, and Kurt Langworthy (CAMCOR) for technical and administrative support in the University of Oregon Electron Microprobe Laboratory. John Donovan created modifications of Probe for EPMA software. John Fournelle and Anette von der Handt provided key inputs into the creation of this software routine. Samples from Nevado de Longaví were supplied by Daniel Sellés. Many people have participated in field and laboratory activities in connection with studies of the five volcanoes included in this investigation. Foremost among those who made the current research possible are Daniel Sellés and Carolina Rodríguez at Nevado de Longaví, Lauren Cooper at Chillán, Caroline Bouvet de Maisonneuve, Jason Jweda, Charlie Langmuir, Alain Burgisser, Daniel Sellés, Steve Turner, Lauren Cooper, Steve Goldstein, (and others) at Lonquimay and Llaima, plus Jon Davidson, Brad Singer, Charlie Langmuir, Ren Thompson, Andrew Wulff, Laurie Brown, Mike Rhodes, (and many others) at Tatara-San Pedro. Dungan extends gratitude to these collaborators.

Suggestions by Domonik Sorger and an anonymous reviewer led to improvements in the paper. We thank Aaron Lussier for editorial handling of this submission.

References

Bacon, C.R. and Hirschmann, M.M. (1988) Mg/Mn partitioning as a test for equilibrium between coexisting Fe-Ti oxides. American Mineralogist, 73(1-2), 57-61.

Borisova, A.Y. (2018) Secondary fluorescence effects in microbeam analysis and their impacts on geospeedometry and geothermometry. Chemical Geology, 490, 22-29.

Bouvet de Maisonneuve, C., Dungan, M.A., Bachmann, O., and Burgisser, A. (2012) Petrological insights into shifts in eruptive styles at Volcán Llaima (Chile). Journal of Petrology, 54, 393-420.

Bullock, E., Locock, A., von der Handt, A., Fournelle, J., Dungan, M., and Donovan, J. (2020) Including the Oxidation State of Iron to Improve Matrix Corrections in EPMA Analyses. Microscopy and Microanalysis, 26(S2), 1876-1877.

Canil, D. and Fedortchouk, Y. (2001) Olivine-liquid partitioning of vanadium and other trace elements, with applications to modern and ancient picrites. Canadian Mineralogist., 39, 319-330.

Costa, F. and Dungan, M.A. (2005) Short time scales of magmatic assimilation from diffusion modeling of multiple elements in olivine. Geology, 33(10), 837-840.

Donovan, J.J. and Tingle, T.N. (1996) An improved mean atomic number background correction for quantitative microanalysis. Microscopy and Microanalysis, 2(1), 1-7.

Donovan, J.J., Singer, J.W, and Armstrong, J.T. (2016) A new EPMA method for fast trace element analysis in simple matrices. American Mineralogist, 101(8), 1839-1853.

Donovan, J.J., Kremser, D., Fournelle, J.H., and Goemann, K. (2021) Probe for EPMA, v. 12.9.5: Users Guide, Acquisition, automation and analysis: Eugene, Oregon, Probe Software. Inc., http://www.probesoftware.com.

Droop, G.T.R. (1987) A general equation for estimating Fe^{3+} concentrations in ferromagnesian silicates and oxides from microprobe analyses, using stoichiometric criteria. Mineralogical Magazine, 51(361), 431-435.

Dungan, M.A., Wulff, A., and Thompson, R. (2001) A refined eruptive stratigraphy for the Tatara-San Pedro Complex (36˚S, Southern Volcanic Zone, Chilean Andes): Reconstruction methodology and implications for magma evolution at long-lived arc volcanic centers. Journal of Petrology, 42, 555-626.

Dungan, M.A. and Davidson, J.P. (2004) Partial assimilative recycling of the mafic plutonic roots of arc volcanoes: An example from the Chilean Andes. Geology, 32, 773-776.

Fournelle, J., Moy, A., Nachlas, W., and Donovan, J. (2020) The EPMA Matrix Correction: All Elements Must Be Present for Accuracy: Four Examples with B, C, O and F. Microscopy and Microanalysis, 26(S2), 58-59.

Frost, B.R. (1991) Introduction to oxygen fugacity and its petrologic importance. in Oxide Minerals: Petrologic and magnetic significance, Reviews in Mineralogy, 25, 1-9.

Ghiorso, M.S. and Evans, B.W. (2008) Thermodynamics of rhombohedral oxide solid solutions and a revision of the Fe-Ti two-oxide geothermometer and oxygen-barometer. American Journal of Science, 308, 957-1039.

Höfer, H.E., and Brey, G. P. (2007) The iron oxidation state of garnet by electron microprobe: Its determination with the flank method combined with major-element analysis. American Mineralogist, 92(5-6), 873-885.

Nash, W.P. (1992) Analysis of oxygen with the electron microprobe: Applications to hydrated glass and minerals. American Mineralogist, 77(3-4), 453-457.

Rodríguez, C., Sellés, D., Dungan, M., Langmuir, C. and Leeman, W. (2007) Adakitic dacites formed by intracrustal crystal fractionation at Nevado de Longaví Volcano (36.2˚S; Andean Southern Volcanic Zone, Central Chile). Journal of Petrology, 48, 2033-2061.

Sack, R.O. and Ghiorso, M.S. (1991a) An internally consistent model for the thermodynamic properties of Fe-Mg titanomagnetite-aluminate spinels. Contributions to Mineralogy and Petrology, 106(4), 474-505.

Sack, R.O. and Ghiorso, M.S. (1991b) Chromian spinels as petrogenetic indicators: Thermodynamic and petrological applications. American Mineralogist, 76(5-6), 827-847.

Schonwalder-Angel, D., Cortés, J.A. and Calder, E.S. (2018) The interplay of magmatism and tectonics: An example based the satellite scoria cones at Llaima, volcano, Chile. Journal of Volcanology and Geothermal Research, 367, 31-45.

Sellés, D., Dungan, M., Langmuir, C., Rodríguez, A.C., and Leeman, W.P. (2022) Magma and mineral composition responses to increasing slab-derived fluid flux: Nevado de Longaví volcano, Southern Chilean Andes. Frontiers in Earth Science, March, 10, article 846997.

Tingle, T.N., Neuhoff, P., Ostergren, J., Jones, R.E., and Donovan, J.J. (1996) The effect of "missing" (unanalyzed) oxygen on quantitative electron probe microanalysis of hydrous silicate and oxide minerals, Abstracts with Programs, Geological Society of America, 28, 212.

Zhang, C., Almeev, R.R., Hughes, E.C., Borisov, A.A., Wolff, E.P., Höfer, H.E., Botcharnikov, R.E., and Koepke, J. (2018) Electron microprobe technique for the determination of iron oxidation state in silicate glasses. American Mineralogist, 103(9), 1445–1454.

Figure Captions

Figure 1: PFE analyses (data reduced with excess-oxygen) plotted against excess-oxygen. Average sub-grain compositions (dark colors) are superimposed on individual data points (pale). The distributions of individual analytical points for any two variables define dense fields that are only slightly broader than corresponding fields for sub-grain averages (~3-5 analyses for a typical average value). Spinel inclusions in pyroxene phenocrysts that are enriched in Mg+Al in comparison to typical groundmass grains (Blocks 4-5-6; green symbols) are discussed in the text, as are Cr-Al spinels that occur as inclusions in olivine (chartreuse, black borders). Labels for "high-fO_2" and "low-fO_2" indicate relative tendencies at the ends of data-arrays, and do not represent absolute values. Compositions of end-member ilmenite, ulvöspinel, and magnetite are shown for reference purposes by yellow rectangles containing red crosses on all three Figures, wherever possible; e.g., ilmenite and ulvöspinel compositions are located at the origins of panels 1c & 1d, where $Fe^{3+}/\Sigma Fe$ and excess-oxygen are zero. Note 'back-projections' of the cubic and rhombohedral arrays toward the origins. The cubic array projects to Fe_3O_4 at excess-oxygen = 6.91 wt% and $Fe^{3+}/\Sigma Fe = 0.667$. Same color and symbol scheme is used in Figures 2 and 3.

Figure 2: End-member compositions in ternary system shown for reference. Note scale changes for FeO wt% between 2c-2d and 2e-2f. Same color and symbol scheme as in Figures 1 and 3.

Figure 3: Note scale-change for ΔTiO_2 in 3c versus 3d. Progressive decreases in ΔTiO_2 above ~16 wt% TiO_2 for spinel in Figure 3d, returned by the PFE calculation, are consistent with the requirements imposed by the ternary substitution scheme. Yellow rectangles with red crosses mark the positions of end-member ilmenite, ulvöspinel, and magnetite compositions (Figure 3d), at which ΔTiO_2 would equal zero. Same color and symbol scheme as in Figures 1 and 2.

This is the peer-reviewed, final accepted version for American Mineralogist, published by the Mineralogical Society of America.
The published version is subject to change. Cite as Authors (Year) Title. American Mineralogist, in press.
DOI: https://doi.org/10.2138/am-2022-8447. http://www.minsocam.org/

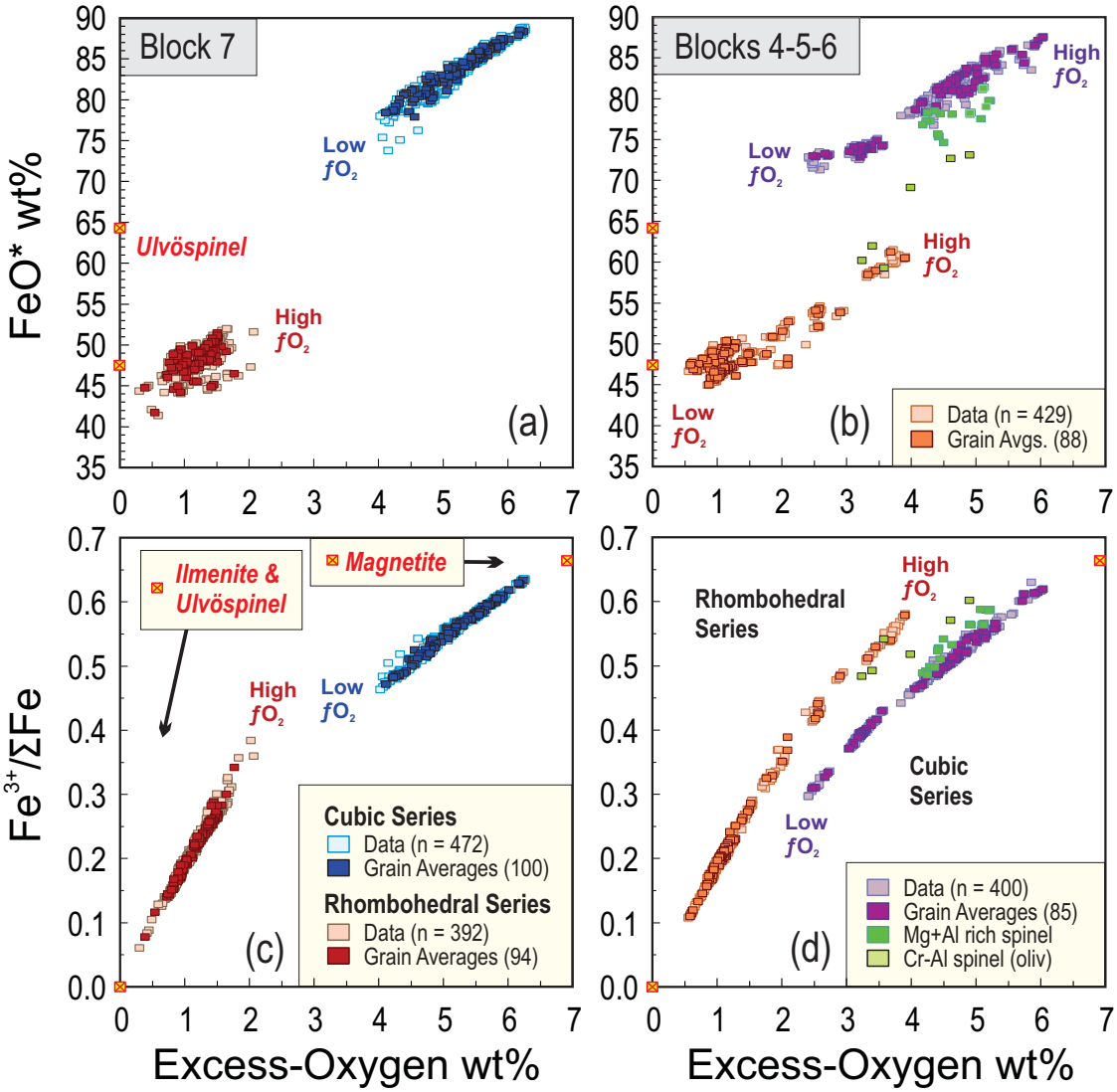

Figure 1: Dungan et al.

This is the peer-reviewed, final accepted version for American Mineralogist, published by the Mineralogical Society of America.
The published version is subject to change. Cite as Authors (Year) Title. American Mineralogist, in press.
DOI: https://doi.org/10.2138/am-2022-8447. http://www.minsocam.org/

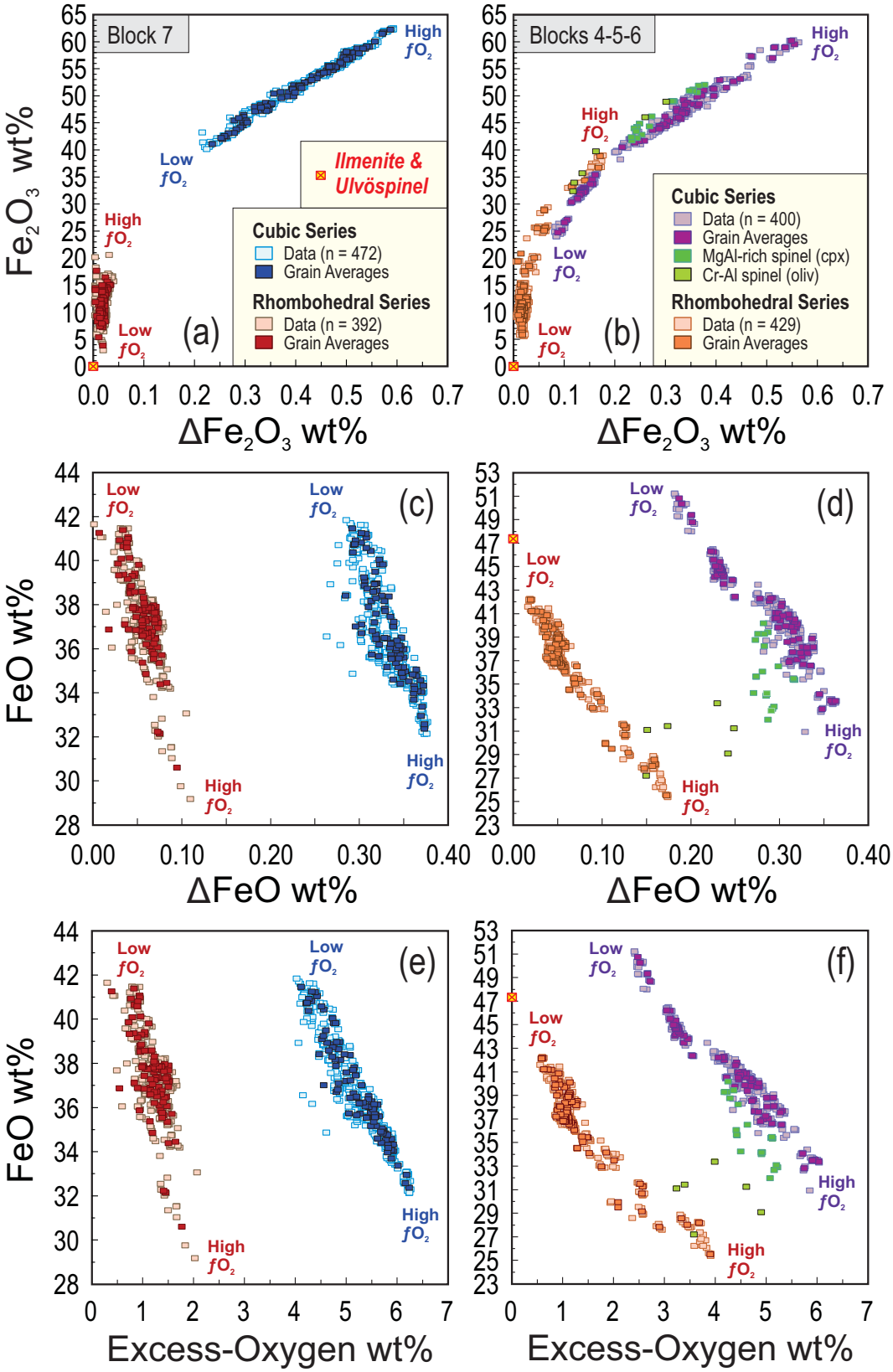

Figure 2: Dungan et al.

This is the peer-reviewed, final accepted version for American Mineralogist, published by the Mineralogical Society of America.
The published version is subject to change. Cite as Authors (Year) Title. American Mineralogist, in press.
DOI: https://doi.org/10.2138/am-2022-8447. http://www.minsocam.org/

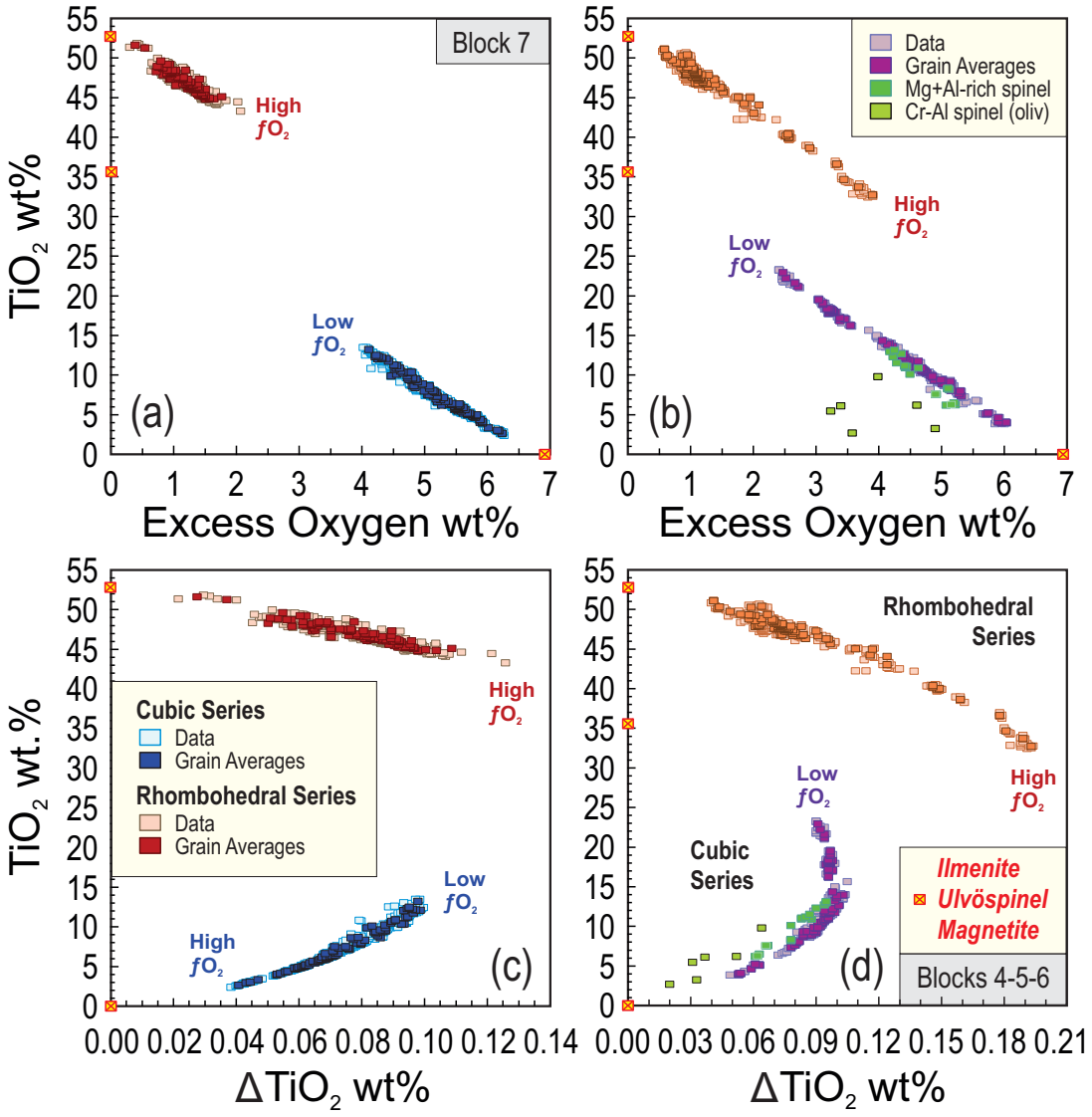

Figure 3: Dungan et al.

This is the peer-reviewed, final accepted version for American Mineralogist, published by the Mineralogical Society of America.
The published version is subject to change. Cite as Authors (Year) Title. American Mineralogist, in press.
DOI: https://doi.org/10.2138/am-2022-8447. http://www.minsocam.org/

Table 1: Electron microprobe analyses of select cubic-rhombohedral pairs

	1	2	3	4	5	6	7	8	9	10	11	12	13	14	15	16
Source	**Lonq.**	*Lonq.*	**Lonq.**	*Lonq.*	**NLV**	*NLV*	**NLV**	*NLV*	**UPSPS**	*UPSPS*	**UPSPS**	*UPSPS*	**UPSPS**	*UPSPS*	**UPSPS**	*UPSPS*
Sample	**LQY-1**	*LQY-1*	**LQY-1**	*LQY-1*	**7143**	*7143*	**7143**	*7143*	**ESPN-8**	*ESPN-8*	**ESPN-8**	*ESPN-8*	**ESPN-9**	*ESPN-9*	**ESPN-9**	*ESPN-9*
Method	**PFE**	*Droop*	**PFE**	*Droop*	**PFE**	*Droop*	**PFE**	*Droop*	**PFE**	*Droop*	**PFE**	*Droop*	**PFE**	*Droop*	**PFE**	*Droop*
Phase	**Mgt (2)**	*Mgt (2)*	**Ilm (2)**	*Ilm (2)*	**Mgt (2)**	*Mgt (2)*	**Ilm (4)**	*Ilm (4)*	**Mgt (4)**	*Mgt (4)*	**Ilm (4)**	*Ilm (4)*	**Mgt (5)**	*Mgt (5)*	**Ilm (5)**	*Ilm (5)*
ID	**Pair-4**	*Pair-4*	**Pair-4**	*Pair-4*	**GMS-3**	*GMS-3*	**GMS-3**	*GMS-3*	**GMS-1**	*GMS-1*	**GMS-1**	*GMS-1*	**GMS-5**	*GMS-5*	**GMS-5**	*GMS-5*
MgO	**1.05**	*1.05*	**1.70**	*1.70*	**0.74**	*0.75*	**2.34**	*2.34*	**0.88**	*0.89*	**2.30**	*2.30*	**1.01**	*1.02*	**3.36**	*3.37*
MnO	**0.71**	*0.70*	**0.84**	*0.84*	**0.21**	*0.20*	**0.44**	*0.44*	**0.28**	*0.27*	**0.55**	*0.54*	**0.36**	*0.35*	**0.86**	*0.86*
V_2O_3	**0.25**	*0.25*	**0.00**	*0.00*	**0.71**	*0.70*	**0.26**	*0.26*	**0.88**	*0.86*	**0.19**	*0.19*	**0.62**	*0.61*	**0.11**	*0.11*
Cr_2O_3	**0.00**	*0.00*	**0.00**	*0.00*	**0.39**	*0.38*	**0.08**	*0.08*	**0.08**	*0.07*	**0.00**	*0.00*	**0.03**	*0.02*	**0.01**	*0.00*
Al_2O_3	**1.10**	*1.11*	**0.07**	*0.07*	**0.79**	*0.80*	**0.06**	*0.06*	**1.57**	*1.58*	**0.08**	*0.08*	**1.30**	*1.31*	**0.07**	*0.11*
SiO_2	**0.12**	*0.12*	**0.03**	*0.03*	**0.08**	*0.08*	**0.04**	*0.04*	**0.09**	*0.08*	**0.05**	*0.05*	**0.09**	*0.08*	**0.10**	*0.10*
CaO	**0.11**	*0.10*	**0.12**	*0.12*	**0.09**	*0.09*	**0.07**	*0.07*	**0.09**	*0.08*	**0.11**	*0.11*	**0.18**	*0.17*	**0.24**	*0.23*
TiO_2	**21.17**	*21.08*	**50.32**	*50.28*	**4.10**	*4.04*	**40.24**	*40.19*	**9.37**	*9.29*	**46.68**	*46.60*	**4.99**	*4.93*	**46.09**	*45.99*
FeO	**48.74**	*48.53*	**41.25**	*41.23*	**33.53**	*33.17*	**31.53**	*31.40*	**38.18**	*37.86*	**37.25**	*37.19*	**34.19**	*33.83*	**34.39**	*34.32*
Fe_2O_3	**27.13**	*27.02*	**6.28**	*6.26*	**58.98**	*58.45*	**25.11**	*25.05*	**47.79**	*47.45*	**12.38**	*12.35*	**58.15**	*57.65*	**15.04**	*15.02*
Total	**100.37**	*99.95*	**100.60**	*100.52*	**99.64**	*98.65*	**100.17**	*99.82*	**99.20**	*98.36*	**99.58**	*99.30*	**100.93**	*99.80*	**100.27**	*100.11*
Wt% excess-O	**2.72**	*0.00*	**0.63**	*0.00*	**5.91**	*0.00*	**2.52**	*0.00*	**4.79**	*0.00*	**1.24**	*0.00*	**5.83**	*0.00*	**1.51**	*0.00*
FeO*	**73.14**	*72.85*	**46.90**	*46.86*	**86.60**	*85.76*	**54.12**	*53.94*	**81.18**	*80.56*	**48.39**	*48.31*	**86.52**	*85.70*	**47.92**	*47.83*
Cations[1]																
Ti	**0.589**	*0.590*	**0.940**	*0.940*	**0.117**	*0.117*	**0.758**	*0.758*	**0.267**	*0.266*	**0.879**	*0.879*	**0.140**	*0.140*	**0.856**	*0.855*
Mg	**0.058**	*0.058*	**0.063**	*0.063*	**0.043**	*0.043*	**0.087**	*0.088*	**0.050**	*0.050*	**0.086**	*0.086*	**0.056**	*0.057*	**0.124**	*0.124*
Mn	**0.022**	*0.022*	**0.018**	*0.018*	**0.006**	*0.007*	**0.009**	*0.009*	**0.009**	*0.009*	**0.012**	*0.012*	**0.012**	*0.011*	**0.018**	*0.018*
V	**0.007**	*0.007*	**0.000**	*0.000*	**0.021**	*0.021*	**0.005**	*0.005*	**0.027**	*0.026*	**0.004**	*0.004*	**0.019**	*0.018*	**0.002**	*0.002*
Cr	**0.000**	*0.000*	**0.000**	*0.000*	**0.012**	*0.012*	**0.002**	*0.002*	**0.002**	*0.002*	**0.000**	*0.000*	**0.001**	*0.001*	**0.000**	*0.000*
Al	**0.048**	*0.048*	**0.002**	*0.002*	**0.036**	*0.036*	**0.002**	*0.002*	**0.070**	*0.071*	**0.002**	*0.002*	**0.057**	*0.058*	**0.002**	*0.002*
Si	**0.004**	*0.004*	**0.001**	*0.001*	**0.003**	*0.003*	**0.001**	*0.001*	**0.003**	*0.003*	**0.001**	*0.001*	**0.003**	*0.003*	**0.002**	*0.002*
Ca	**0.003**	*0.004*	**0.003**	*0.003*	**0.004**	*0.004*	**0.002**	*0.002*	**0.004**	*0.003*	**0.003**	*0.003*	**0.007**	*0.007*	**0.006**	*0.006*
Fe^{2+}	**1.510**	*1.510*	**0.857**	*0.857*	**1.068**	*1.067*	**0.660**	*0.660*	**1.208**	*1.207*	**0.780**	*0.780*	**1.069**	*1.069*	**0.710**	*0.710*
Fe^{3+}	**0.756**	*0.756*	**0.117**	*0.117*	**1.690**	*1.691*	**0.474**	*0.474*	**1.361**	*1.361*	**0.233**	*0.233*	**1.636**	*1.636*	**0.279**	*0.280*
Fe*	**2.266**	*2.266*	**0.974**	*0.974*	**2.757**	*2.758*	**1.134**	*1.134*	**2.569**	*2.568*	**1.013**	*1.013*	**2.704**	*2.704*	**0.989**	*0.989*
Fe^{3+}/ΣFe	**0.334**	*0.334*	**0.120**	*0.120*	**0.613**	*0.613*	**0.417**	*0.417*	**0.530**	*0.530*	**0.230**	*0.230*	**0.605**	*0.605*	**0.282**	*0.282*
Log (Mg/Mn)	**0.42**	*0.42*	**0.55**	*0.55*	**0.79**	*0.79*	**0.97**	*0.97*	**0.74**	*0.74*	**0.87**	*0.87*	**0.69**	*0.69*	**0.84**	*0.84*
	fO_2, Fe-Ti / Fe-Mg		**ΔNNO = -1.35, 865/1262˚C**		**ΔNNO = 1.58, 696/636˚C**		**ΔNNO = 0.27, 792/773˚C**		**ΔNNO = 0.93, 680/605˚C**							
	fO_2, Fe-Ti / Fe-Mg		*ΔNNO = -1.35, 865/1267˚C*		*ΔNNO = 1.58, 695/650˚C*		*ΔNNO = 0.27, 792/792˚C*		*ΔNNO = 0.93, 680/615˚C*							

Comparisons of data from oxide pairs in four samples: (LQY-1, columns 1-4) Historic andesitic lava from Lonquimay volcano, (7143, columns 5-8, 38.45˚S) Holocene andesitic lava from east flank of Nevado de Longaví volcano (NLV, 36.2˚S), and (ESPN-8 & ESPN-9, columns 9-16) Basaltic lavas of the Upper Placeta San Pedro sequence (UPSPS) of the Tatara-San Pedro complex (TSPC, 36˚S). Numbers of analyses used to compute the averages for each sub-grain in parentheses. Cubic and rhombohedral phases are referred to as Mgt and Ilm respectively, due to space considerations. Odd-numbered columns (**PFE - Bold**) present results that are fully reduced, such that excess oxygen is incorporated into matrix corrections. Even-numbered columns (*Droop - Italics*) present the same data without consideration of excess-oxygen during data-reduction. Ferric and ferrous iron in the latter have been calculated by the Droop Method *following* data reduction. Oxide values that change significantly due to excess-oxygen are underlined. [1]Cation proportions (pfu) in both schemes are calculated on the basis of charge balance and stoichiometry, with 3 total cations and 4 oxygens for spinel, and 2 total cations and 3 oxygens for the rhombohedral phase. Despite different total-iron contents (FeO*), as well as different FeO wt% and Fe_2O_3 wt% returned by the two data-reduction methods, the imposition of total-cation and oxygen normalization to the same analytical data leads to identical values of Fe*, Fe^{2+}, Fe^{3+}, and Fe^{3+}/ΣFe. These, in turn, lead to essentially identical estimates of oxygen fugacity (ΔNNO) and Fe-Ti equilibration temperatures. Fe-Mg equilibration temperatures vary. The Ghiorso and Evans (2008) algorithm applies the Droop normalization-method to input data, prior to calculation of T-fO_2.